Energy-Efficient Neuromorphic Closed-Loop Modulation System for Parkinson's Disease

Abstract— **Parkinson's Disease (PD) impacts millions globally, causing debilitating motor symptoms. While Closed-Loop Deep Brain Stimulation (CL-DBS) has emerged as a promising treatment, existing systems often suffer from high energy consumption, making them impractical for wearable or implantable devices. This research introduces an innovative neuromorphic approach to enhance CL-DBS performance, utilizing Leaky Integrate-and-Fire (LIF) neuron-based controllers to adaptively modulate stimulation signals based on symptom severity. Two controller designs, the on-off LIF and dual LIF models, are proposed, achieving significant reductions in power consumption by 19% and 56%, respectively, while enhancing suppression efficiency by 4.7% and 6.77%. Additionally, this work addresses the scarcity of datasets for PD symptoms by developing a novel dataset featuring neural activity from the subthalamic nucleus (STN), incorporating beta oscillations as key physiological biomarkers. This dataset aims to support further advancements in neuromorphic CL-DBS systems and is openly shared with the research community. By combining energy-efficient neuromorphic controllers with a comprehensive dataset, this study not only advances the technological feasibility of CL-DBS systems for PD treatment but also provides a foundation for personalized and adaptive neuromodulation therapies, paving the way for improved quality of life for individuals with Parkinson's Disease.**

Keywords— Parkinson's Disease, Closed-Loop Deep Brain Stimulation, Neuromorphic Computing.

I. Introduction

Parkinson's Disease (PD) affects millions of individuals globally each year, posing significant challenges in both diagnosis and management [1]. Although pharmaceutical treatments are commonly employed to alleviate PD symptoms, their long-term efficacy declines due to the development of drug resistance. Consequently, patients in advanced stages often require higher doses, which can result in adverse effects such as depression and speech impairments [1]. Deep Brain Stimulation (DBS) has emerged as a promising therapeutic alternative, offering symptom relief through continuous electrical pulses delivered via electrodes implanted in the brain. These electrodes are surgically placed through small cranial openings, while the stimulation signals are generated and modulated by a device implanted in the patient's chest.

However, traditional DBS systems deliver fixed stimulation patterns regardless of the patient's clinical state, often leading to unwanted side effects. Additionally, the constant nature of these stimulation signals accelerates battery depletion, necessitating frequent surgical interventions for device replacement [2]. To address these limitations, the Closed-Loop DBS (CL-DBS) system has been proposed. This advanced system optimizes stimulation by tailoring it to the patient's specific symptoms, leveraging physiological biomarkers such as beta oscillations (13–30 Hz) in the subthalamic nucleus (STN) for real-time adjustments. Despite the promise of CL-DBS in improving therapeutic outcomes, its adoption is hindered by significant challenges, particularly in terms of power consumption [3, 4]. Unlike traditional open-loop DBS (OL-DBS) systems, which deliver continuous or pre-programmed stimulation, CL-DBS requires real-time monitoring and dynamic adjustment of stimulation parameters based on physiological signals. This functionality involves continuous neural signal processing and rapid computational feedback loops, resulting in substantially higher energy demands. Current implementations of CL-DBS systems rely on sophisticated yet computationally intensive algorithms and hardware platforms, such as reinforcement learning [2, 5], fuzzy inference systems [6], field-programmable gate arrays (FPGAs) [2], and Artificial Neural Networks (ANNs) [7]. While these approaches enhance the precision and adaptability of the stimulation, their energy inefficiency limits their feasibility for use in implanted medical devices. Addressing this critical issue is essential for realizing the full potential of CL-DBS systems in clinical applications.

This paper presents a novel neuromorphic closed-loop deep brain stimulation (CL-DBS) system that employs the Leaky Integrate-and-Fire (LIF) neuron model as a dynamic controller for stimulation signals. To meet the growing data requirements of neuromorphic methodologies, we have also

developed a specialized Parkinson's disease dataset, which includes both raw neural activity and beta-band oscillations from the subthalamic nucleus (STN). The key contributions of our work are summarized as follows:

1) Development of a Comprehensive Parkinson's Disease Dataset: We constructed a computationally modeled dataset featuring beta oscillation signals from the STN and the Globus Pallidus internus (GPi). These signals serve as critical electrophysiological biomarkers for Parkinson's disease, enabling more effective neuromorphic system designs.
2) Design and Implementation of LIF-Based Neuromorphic Controllers: We propose and implement several LIF-based controllers for the neuromorphic CL-DBS system, designed to dynamically regulate the amplitude of DBS stimulation signals. Our novel controllers—namely, the on-off LIF controller and the dual LIF controller—demonstrate significant advancements in performance. Specifically, on-off LIF controller achieves a 19% reduction in power consumption, while enhancing suppression efficiency by 4.7%.and dual LIF controller achieves a 56% reduction in power consumption, with a corresponding improvement in suppression efficiency of 6.77%.

II. Concepts and Advances in Closed-Loop Deep Brain Stimulation for Parkinson's Disease

The traditional Deep Brain Stimulation (DBS) systems, as illustrated in Figure 1(a), utilize fixed electric square waveform pulses to target specific brain regions, particularly the basal ganglia, to alleviate motor symptoms in Parkinson's disease (PD) patients. The basal ganglia, a critical part of the motor control circuitry, contain key structures like the subthalamic nucleus (STN) and globus pallidus internus (neurostimulation as primary targets for DBS. These systems typically involve implanting electrodes into these brain regions, which are connected to an implantable pulse generator (IPG) via an insulated wire threaded beneath the patient's skin and placed subcutaneously, often in the upper chest. This arrangement allows for continuous stimulation aimed at treating various movement disorders, such as Parkinson's disease, dystonia, and essential tremors [8].

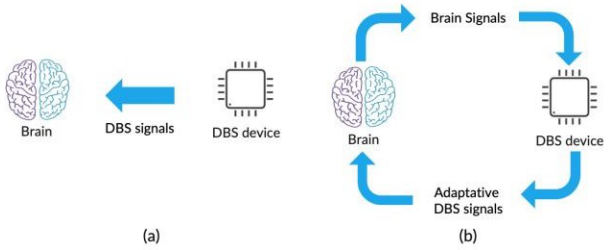

Figure 1: (a) Open-Loop DBS; (b) Closed-Loop DBS.

Conventional DBS systems function in a one-directional, open-loop (OL) configuration, delivering continuous stimulation based on predefined parameters without considering the patient's real-time physiological state or variations in symptom severity. While this approach has been effective in reducing PD symptoms, it presents notable drawbacks, including excessive battery consumption and the potential for adverse side effects due to unregulated stimulation. Since the system operates without dynamic feedback, it lacks the ability to tailor stimulation parameters in response to changes in the patient's neurological state, limiting its therapeutic efficacy and energy efficiency.

To overcome the limitations of OL-DBS systems, a novel concept known as closed-loop DBS (CL-DBS) has been introduced. Unlike its predecessor, CL-DBS incorporates a real-time feedback mechanism that continuously monitors physiological signals or biomarkers from the brain, enabling dynamic adjustments to stimulation parameters. Figure 1 illustrates the key differences between OL-DBS and CL-DBS. This adaptive framework ensures that DBS therapy can respond to changes in neural activity or symptom severity, thereby improving overall treatment effectiveness. The CL-DBS system's ability to automatically modify stimulation parameters without user intervention represents a substantial advancement in personalized treatment, offering the potential for more precise symptom management.

III. Building Dataset of Parkinson's Disease using a Computional Model

The data scarcity poses a severe issue for the neuromorphic community when applying Spiking Neural Networks (SNNs) and neuromorphic algorithms to medical applications. To address this challenge, we are building a novel dataset of PD biomarkers using a computational model [9].

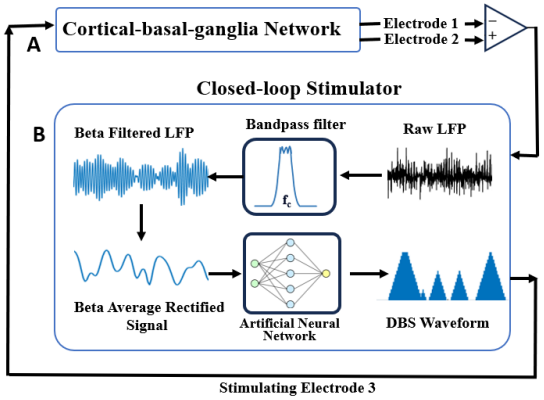

Figure 2: Diagram of Closed-loop DBS System: (A) Network diagram of cortical basal ganglia neuron populations; (B) Diagram of the closed-loop stimulator [9].

The computational model for building the PD dataset is illustrated in Figure 2. The computation model consists of an extracellular DBS electric field and simulation of the local field potentials (LFP) at STN that is formed between the cortex, basal ganglia, and thalamus [10].

The data is generated from the cortico-basal ganglia computational model, represented as raw local field

potentials (LFP) [9]. Local Field Potential refers to the electrical activity recorded from a small group of neurons in the brain. Unlike single-neuron recordings, which focus on the activity of individual neurons, LFP recordings capture the combined activity of nearby neurons. LFP recordings are usually obtained using electrodes implanted in the brain tissue. In the computational model used for building the PD dataset, these electrodes detect the electrical fluctuations generated by the synchronized activity of a population of neurons between the cortex, STN, and thalamus.

The main components of the model are interneurons and cortical neurons of the cortex, STN, globus pallidus externa (GPe), globus pallidus interna (GPi), and thalamus neurons. Cortical pyramidal neurons are simulated using conductance-based biophysical models enabling extracellular DBS electric field to cortical axons. AMPA and GABA imply excitatory synapses and inhibitory synapses respectively. A total of six hundred STN, GPe, GPi, thalamic, cortical interneuron, and cortical pyramidal neurons are connected through these excitatory and inhibitory synapses which are illustrated in Figure 3. The connectivity pattern between neurons in the cortico-basal ganglia network is random. Each of the STN neurons receives 5 inhibitory inputs from GPe neurons and excitatory inputs from five cortical neurons [11]. Each globus pallidus externus (GPe) neuron is subjected to inhibitory input from one striatal neuron and one other GPe neuron while receiving excitatory input from two subthalamic nucleus (STN) neurons. Conversely, each globus pallidus internus (GPi) neuron receives excitatory input from a single STN neuron and inhibitory input from a single GPe neuron. Thalamic neurons encounter inhibitory input from a GPi neuron. Cortical neurons are stimulated by excitatory input from one thalamic neuron and concurrently inhibited by input from ten interneurons. In turn, interneurons are activated by excitatory input from ten cortical neurons [12].

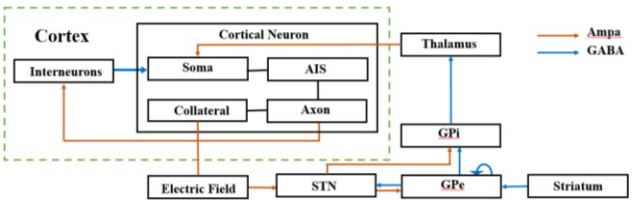

Figure 3: Diagram of cortical basal ganglia network.

The cortex is comprised of interneurons and cortical pyramidal neurons. The cortical neuron model consists of soma, axon initial segment (AIS), main axon, and axon collateral. These cortical neuron soma and interneuron models are generated based on regular spiking models. Subthalamic Nucleus includes a leak, sodium, three potassium, two calcium ionic currents, and an intracellular bias current for setting the neuron firing rate. STN plays a vital role in generating bursting activity during Parkinson's disease.

The models for both globus pallidus externus (GPe) and internus (GPi) neurons consist of leak, sodium, two potassium, and two calcium ionic currents, alongside an intracellular bias current that regulates the neuron firing rates. In the case of GPe neurons, an additional intracellular current is introduced to replicate DBS application, with the assumption that a proportionate number of GPe neurons are stimulated as compared to extracellularly stimulated cortical neurons during DBS. Thalamic neurons are also modeled similarly, though one calcium and one potassium current are excluded. The synaptic input from the striatum to GPe neurons is modeled as a collection of Poisson-distributed spike trains operating at a frequency of 3 Hz. The acquired raw LFP is shown in the following Figure 4.

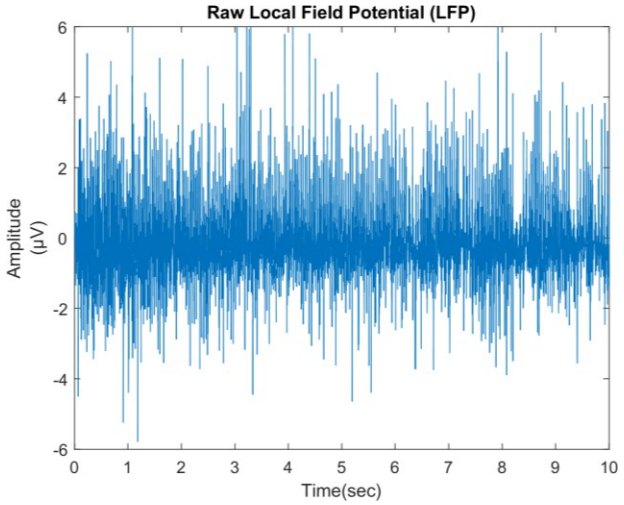

Figure 4: Raw local field potential generated from the neuron population between cortex, STN, and thalamus.

These raw signals of LFP are recorded by the contact electrodes 1 and 2 followed as shown in Figure 2. This is estimated as the summation of the extracellular potentials due to the spatially distributed synaptic currents across the STN population. A bandpass filter is applied to acquire the beta-band filtered LFP.

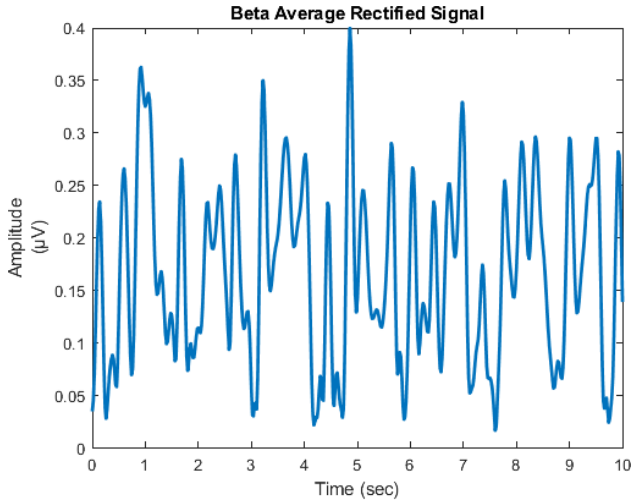

Figure 5: Beta Average Rectified Signal.

The average rectified value (ARV) of the beta-band LFP is calculated by full-wave rectifying the filtered LFP signal

using a fourth-order Chebyshev band-pass filter with an 8 Hz bandwidth, centered about the peak in the LFP power spectrum. The acquired Beta Average rectified signal (ARV) can be seen in Figure 5.

IV. Leaky-and-Fire Neuron Controller Design for a Neuromorphic Closed-Loop Deep Brain Stimulation System.

Two neuromorphic controllers, designed specifically for Closed-Loop Deep Brain Stimulation (CL-DBS) systems, are proposed based on the Leaky Integrate-and-Fire (LIF) neuron model. These controllers, named the on-off LIF and dual-threshold LIF controllers, aim to regulate the power density of beta oscillations in the subthalamic nucleus (STN) by adjusting the input DBS currents to achieve a defined target value. The LIF neuron models provide the foundation for implementing these controllers. The on-off LIF controller operates by comparing the Beta Average Rectified Value (ARV) to a predefined target and modulating the DBS current accordingly. The DBS current ranges between a minimum of 0 mA and a maximum of 3 mA. When the Beta ARV exceeds the target, the DBS current (I_{DBS}) increases, but it remains constant when the Beta ARV is below the target. Within the LIF model, when the membrane potential surpasses the threshold voltage (V_{th}), the neuron fires, resetting the membrane potential to V_{leak}. The Beta ARV is compared against the membrane potential, and the target value is compared to the threshold voltage. Adjustments to the DBS current are based on the following equations:

$$\frac{dv}{dx} = \frac{\{-(Beta\ ARV - b_{target}) + RI\}}{\tau_m}, \quad (1)$$

$$I_{DBS} = \frac{dy}{dx}/R, \quad (2)$$

where τ_m is the membrane time constant, R is the membrane resistance, and $I(t)$ represent the input current to the neuron. The specific parameters for the on-off LIF controller are listed in Table 1.

Table 1: Parameters of On-Off LIF DBS Controller

$V_m(t)$	V_{th}	τ_m	R	I	b_{target}
Measured Beta ARV	b_{target}	5	0.5 Ω	5 mA	0.104 µV

When the Beta ARV remains below the target, the DBS current does not change. The simulation results are shown in Figure 6. Beta oscillations were derived from raw Local Field Potential (LFP) data, and the Beta ARV was calculated by rectifying the filtered LFP signal with a fourth-order Chebyshev band-pass filter, centered on an 8 Hz bandwidth at the peak of the LFP power spectrum. Between 11 and 12 seconds, the DBS current remains constant, as the Beta ARV is below the target. Before 11 seconds, the Beta ARV exceeds the target, causing an upward adjustment in the DBS current. The DBS current remains within the defined limits of 0 mA and 3 mA.

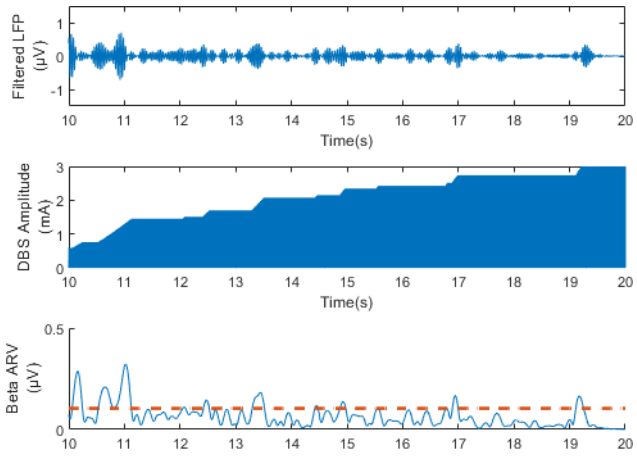

Figure 6: Adaptive DBS current of on-off LIF controller.

The dual-threshold LIF controller uses the same governing equations (Eq. 1 and Eq. 2) as the on-off model but introduces two distinct target thresholds for more precise control. The upper target is set at 0.104 µV, and the lower target is 0.05207 µV, as shown in Table 2. If the Beta ARV exceeds the upper target, the DBS current increases. Conversely, when the Beta ARV falls below the lower target, the DBS current decreases. If the Beta ARV lies between the two thresholds, the DBS current remains unchanged. Figure 7 demonstrates the output behavior of the dual-threshold LIF controller.

Table 2: Parameters of Dual LIF DBS Controller

$V_m(t)$	V_{th}	τ_m	R	I	*Targets* (µV)
Measured Beta ARV	*Targets*	5	0.5 Ω	5 mA	t_{up}= 0.104 t_{low}= 0.05207

The performance of these LIF-based neuromorphic controllers is evaluated based on three essential parameters: mean squared error (MSE), power consumption, and suppression efficiency. Each parameter is critical in determining the overall effectiveness and feasibility of the controllers, especially for applications requiring precision and energy efficiency.

The mean squared error (MSE) quantifies the controllers' ability to maintain the target beta level, providing a numerical measure of accuracy. The MSE is calculated using the following equations:

$$e(t) = \frac{b_{measured} - b_{target}}{b_{target}}, \quad (3)$$

$$MSE = \frac{1}{T_{sim}} \int_0^{T_{sim}} e(t)^2\, dt, \quad (4)$$

where T_{sim} represents the simulation duration, set at 30 seconds. The term $e(t)$ refers to the normalized error signal calculated as the difference between the measured beta ARV and the target beta ARV, normalized by the target beta ARV. MSE values for all controllers are benchmarked against the baseline error observed when DBS is deactivated. This baseline serves as a point of comparison to highlight the improvements achieved by each controller.

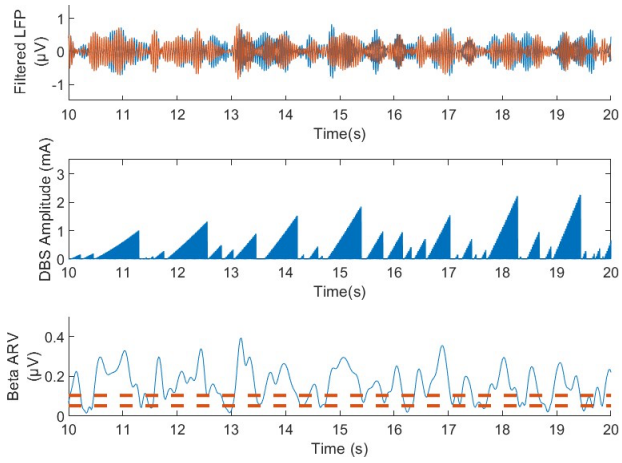

Figure 7: Adaptive DBS current of dual LIF controller.

Figure 8 illustrates the MSE for different CL-DBS controllers, including the open-loop, on-off LIF, and dual LIF controllers.

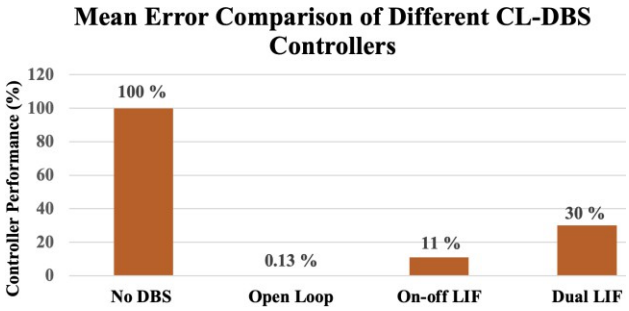

Figure 8: Comparison of mean squared error (MSE) among different CL-DBS controllers.

In the absence of DBS stimulation, the beta ARV signal reflects unregulated pathological beta activity, resulting in a maximum error of 100%. By contrast, when DBS is active, the MSE decreases as the controllers regulate the beta ARV closer to the desired target. Among the controllers tested, the on-off LIF model achieves an MSE of 11%, significantly lower than the 30% observed for the dual LIF model, indicating more effective beta oscillation suppression.

Power consumption is another critical factor, especially for implantable systems that rely on limited battery capacity. The power consumption for each controller is calculated using the formula:

$$Power\ Comsumption = \frac{1}{T_{sim}} \int_0^{T_{sim}} Z_E(t) I_{DBS} t^2\, dt, \quad (5)$$

where Z_E represents electrode impedance (set at 0.5 kΩ), I_{DBS} (t) denotes the DBS current, and T_{sim} is the simulation duration. Figure 9 provides a comparative analysis of power consumption among the different controllers. The results are normalized with respect to the open-loop controller, which uses a constant DBS current of 2.5 mA. The open-loop controller exhibits the highest power consumption at 100%, a direct result of its continuous and unmodulated current application.

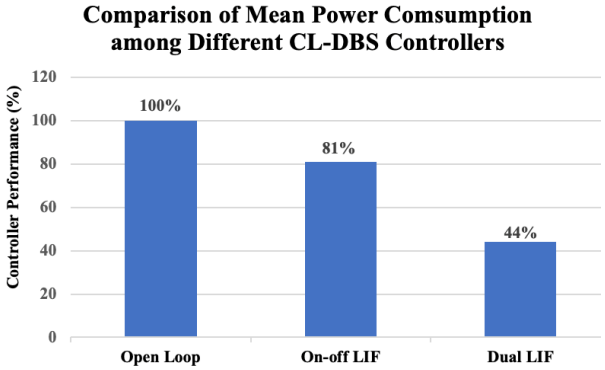

Figure 9: Comparison of the mean power consumption among different CL-DBS controllers.

By comparison, the on-off LIF controller reduces power consumption to 81% of the baseline, while the dual LIF controller achieves the most significant improvement, consuming just 44% of the power used by the open-loop controller. This substantial reduction demonstrates the efficiency of the dual LIF model in managing power usage without compromising performance. The final evaluation metric, suppression efficiency, measures how effectively a controller suppresses beta oscillations per unit of power consumed. This metric is expressed as a percentage per microwatt (%/μW) and is calculated using the formula:

Suppression Efficiency

$$= 100 \times \frac{1 - \frac{1}{T_{sim}} \int_0^{T_{sim}} \frac{b_{DBSOff}(t) - b_{controller}(t)}{b_{DBSOff}(t)} dt}{Power\ Consumption}, \quad (6)$$

where, b_{DBSOFF} refers to the beta ARV signal recorded during the simulation when DBS is inactive, $b_{controller}$ represents the beta ARV signal recorded with the controller in operation. The power consumption is determined by the energy utilized by the controller, as specified in Equation (5). Excessive beta oscillations are a characteristic feature in the basal ganglia of Parkinson's patients [13], contributing to their motor symptoms. Various controllers are designed to mitigate these oscillations by targeting specific beta levels. A controller's effectiveness in managing beta ARV signals improves with higher suppression efficiency, reflecting its ability to regulate abnormal neural activity more precisely.

As shown in Figure 10, suppression efficiency is inversely proportional to power consumption. The open-loop controller, which consumes the most power, achieves the lowest suppression efficiency at just 1.8%/μW. The on-off LIF controller demonstrates a significant improvement with an efficiency of 6.5%/μW, more than three times higher than the open-loop model. However, the dual LIF controller outperforms both, achieving the highest suppression efficiency of 8.57%/μW, confirming its superior capability to balance beta oscillation suppression with minimal power usage.

V. Conclusion

This research introduces a novel neuromorphic approach leveraging LIF-based controllers to adaptively modulate CL-DBS signals based on Parkinson's Disease symptom severity. The on-off LIF and dual LIF controllers presented in this study effectively address critical limitations of existing systems. Specifically, the proposed controllers reduce power consumption by 19% and 56%, respectively, compared to conventional models, while enhancing suppression efficiency by 4.7% and 6.77%. In addition, recognizing the scarcity of Parkinson's Disease datasets, this study contributes a newly curated dataset featuring neural activity from the subthalamic nucleus (STN) at beta oscillations. This dataset, encompassing key biomarkers for Parkinson's diagnosis and therapy, is made publicly available to support further research in neuromorphic computing and CL-DBS development. It can be accessed at https://github.com/Brain-Inspired-AI-Lab/Parkinson-Electrophysiological-Signal-Dataset-PESD.

Acknowledgment

This work was supported by the program: XXX.

References

[1] N. Hwynn, C. J. Hass, P. Zeilman, J. Romrell, Y. Dai, S. S. Wu, K. D. Foote, S. Subramony, G. Oyama, and F. Velez-Lago, "Steady or not following thalamic deep brain stimulation for essential tremor," *Journal of neurology,* vol. 258, pp. 1643-1648, 2011.

[2] Q. Gao, M. Naumann, I. Jovanov, V. Lesi, K. Kamaravelu, W. M. Grill, and M. Pajic, "Model-based design of closed loop deep brain stimulation controller using reinforcement learning," in *2020 ACM/IEEE 11th International Conference on Cyber-Physical Systems (ICCPS)*, 2020: IEEE, pp. 108-118.

[3] Z. Kerman, C. Yu, and H. An, "Beta oscillation detector design for closed-loop deep brain stimulation of Parkinson's disease with memristive spiking neural networks," in *2022 23rd International Symposium on Quality Electronic Design (ISQED)*, 2022: IEEE, pp. 1-6.

[4] N. Zins, Y. Zhang, C. Yu, and H. An, "Neuromorphic computing: A path to artificial intelligence through emulating human brains," in *Frontiers of Quality Electronic Design (QED) AI, IoT and Hardware Security*: Springer, 2023, pp. 259-296.

[5] M. Lu, X. Wei, Y. Che, J. Wang, and K. A. Loparo, "Application of reinforcement learning to deep brain stimulation in a computational model of Parkinson's disease," *IEEE Transactions on Neural Systems and Rehabilitation Engineering,* vol. 28, no. 1, pp. 339-349, 2019.

[6] C. Camara, K. Warwick, R. Bruña, T. Aziz, F. Del Pozo, and F. Maestú, "A fuzzy inference system for closed-loop deep brain stimulation in Parkinson's disease," *Journal of medical systems,* vol. 39, pp. 1-11, 2015.

[7] L. Chen, Z. Ge, and W. Jiang, "Neural network-based closed-loop deep brain stimulation for modulation of pathological oscillation in Parkinson's disease [J]," *IEEE Access,* vol. 8, pp. 161067-161079, 2020.

[8] M. A. B. Siddique, Y. Zhang, and H. An, "Monitoring time domain characteristics of Parkinson's disease using 3D memristive neuromorphic system," *Frontiers in computational neuroscience,* vol. 17, p. 1274575, 2023.

[9] J. E. Fleming, E. Dunn, and M. M. Lowery, "Simulation of closed-loop deep brain stimulation control schemes for suppression of pathological beta oscillations in Parkinson's disease," *Frontiers in neuroscience,* vol. 14, p. 166, 2020.

[10] A. Nambu, H. Tokuno, and M. Takada, "Functional significance of the cortico–subthalamo–pallidal 'hyperdirect'pathway," *Neuroscience research,* vol. 43, no. 2, pp. 111-117, 2002.

[11] M. D. Bevan, C. Francis, and J. Bolam, "The glutamate-enriched cortical and thalamic input to neurons in the subthalamic nucleus of the rat: convergence with GABA-positive terminals," *Journal of Comparative Neurology,* vol. 361, no. 3, pp. 491-511, 1995.

[12] A. M. Packer, D. J. McConnell, E. Fino, and R. Yuste, "Axo-dendritic overlap and laminar projection can explain interneuron connectivity to pyramidal cells," *Cerebral cortex,* vol. 23, no. 12, pp. 2790-2802, 2013.

[13] Z. Yin, R. Ma, Q. An, Y. Xu, Y. Gan, G. Zhu, Y. Jiang, N. Zhang, A. Yang, and F. Meng, "Pathological pallidal beta activity in Parkinson's disease is sustained during sleep and associated with sleep disturbance," *Nature Communications,* vol. 14, no. 1, p. 5434, 2023.